Crystal structure and band gap determination of HfO2 thin films

Marie Cheynet, Simone Pokrant, Frans Tichelaar, Jean-Luc Rouvière

Crystal structure and band gap determination of HfO_2 thin films

Marie C. Cheynet[a),b)]
Laboratoire de Thermodynamique et Physico-Chimie Métallurgiques associated to INPG-CNRS-UJF, ENSEEG BP 75, Saint-Martin d'Hères 38402, France

Simone Pokrant[a),c)]
Philips Semiconductors, 860 Rue Jean Monnet, 38920 Crolles, France

Frans D. Tichelaar
Kavli Institute of Nanoscience, Delft University of Technology, Lorentzweg 1, 2628 CJ Delft, The Netherlands and National Centre for HREM, Delft University of Technology, Lorentzweg 1, 2628 CJ Delft, The Netherlands

Jean-Luc Rouvière
Département de Recherche Fondamentale sur la Matière Condensée, CEA Grenoble, Avenue des Martyrs, 38041 Grenoble Cedex, France

(Received 7 February 2006; accepted 5 January 2007; published online 1 March 2007)

Valence electron energy loss spectroscopy (VEELS) and high resolution transmission electron microscopy (HRTEM) are performed on three different HfO_2 thin films grown on Si (001) by chemical vapor deposition (CVD) or atomic layer deposition (ALD). For each sample the band gap (E_g) is determined by low-loss EELS analysis. The E_g values are then correlated with the crystal structure and the chemical properties of the films obtained by HRTEM images and VEELS line scans, respectively. They are discussed in comparison to both experimental and theoretical results published in literature. The HfO_2 ALD film capped with poly-Si exhibits the largest band gap ($E_g=5.9\pm0.5$ eV), as a consequence of its nanocrystallized orthorhombic structure. The large grains with a monoclinic structure formed in the HfO_2 ALD film capped with Ge and the carbon contamination induced by the precursors in the HfO_2 CVD film capped with Al_2O_3 are identified to be the main features responsible for lower band gap values ($E_g=5.25\pm0.5$ and 4.3 ± 0.5 eV respectively). © *2007 American Institute of Physics*. [DOI: 10.1063/1.2697551]

I. INTRODUCTION

With the downscaling of advanced metal oxide semiconductor field effect transistors (MOSFETs), the SiO_2 gate oxide becomes too thin (<2 nm) to prevent leakage currents resulting from tunnel effects.[1] This integration problem can be solved by using materials with a higher dielectric constant ($\varepsilon > \varepsilon_{SiO_2} \sim 3.5$), since high k oxides can grow thicker (3–5 nm), while maintaining standard device parameters, e.g., threshold voltage (V_t). Among high k materials, IV-B metal oxides and, particularly, hafnium dioxide (HfO_2) are reported to exhibit attractive properties to replace SiO_2: good compatibility with polysilicon, high dielectric constant ($\varepsilon \sim 22$), and relatively wide band gap[1] ($E_g \sim 5.7$ eV). Ideally, dielectric thin films for industrial applications should be amorphous to prevent leakage paths along grain boundaries and should have sharp interfaces with the Si substrate and the gate material. Therefore, as a function of the process (deposition and postdeposition conditions), the chemistry and crystal structure obtained in the HfO_2 thin films can be far from the expected stoichiometry and structural state. Indeed, the complex and numerous deposition steps can lead to thickness variations, chemical composition deviations from the ideal stoichiometry, interfacial roughness, phase formation at the interface with the gate material, and different degrees of crystallinity with various grain sizes and crystal structures. Obviously, all these morphological, structural, and chemical defects can have direct impact on the electronic properties and the leakage current. This means that morphology, crystal structure, and chemical composition of the film and of its interfaces have to be monitored at the same scale as the electronic properties to establish a correlation between both. Analytical transmission electron microscopy (TEM) is the only technique available to give chemical, structural, and physical information in a single experiment with a nanometer scale spatial resolution. In this context several EELS studies on semiconductor structures (HfO_2 and SiO_2) have been already performed; most of them are focused on core edge analysis,[2–4] i.e., intensity and near edge fine structures, to identify chemical and bonding variations across gate oxides. Only few publications[5–7] based on low-loss analysis exist, but none of these low-loss studies provide an exhaustive quantitative analysis leading to a correlation of chemical and physical properties of thin gate oxides.

In this work, we have performed valence electron energy loss spectroscopy (VEELS) and high resolution transmission electron microscopy (HRTEM) in scanning transmission electron microscopy (STEM) and TEM modes, respectively, to investigate different HfO_2 thin films (~4 nm) deposited on Si/SiO_2 substrates by either chemical vapor or atomic layer deposition (CVD-ALD) and then capped with poly-Si,

[a)]Authors to whom correspondence should be addressed.
[b)]Electronic mail: marie.cheynet@ltpcm.inpg.fr
[c)]Electronic mail: simone.pokrant@philipscrolls.st.com

poly-Ge, or poly-Al_2O_3. For each sample, the band gap (E_g) is determined by analyzing low-loss spectra. The values obtained in the different cases are correlated to the chemical profiles across the dielectric HfO_2 layer obtained from the VEELS line-scan analysis and to the microstructure and structural properties determined by high resolution electron microscopy (HREM) imaging.

II. MATERIALS AND METHODS

Three different HfO_2 thin films with a target thickness of 4 nm are studied. In samples 1 and 2 the HfO_2 films are deposited by ALD on a chemically oxidized (001) Si substrate and annealed at 450 and 500 °C, respectively. They are capped with poly-Si (sample 1) or with poly-Ge (sample 2). Sample 3 consists of a $Si/SiO_2/HfO_2/poly\text{-}Al_2O_3$ stack, where the HfO_2 film is deposited by CVD on a chemically oxidized (001) Si substrate. Thin cross sections for TEM experiments are prepared from the full sheet wafers by tripod polishing or sawing followed by focused ion beam (FIB) thinning. The FIB thinning is performed at high energy (30 keV) followed by a cleaning step at low energy (5 keV) to minimize surface amorphization effects. TEM thin foil thicknesses are around 50 ± 5 nm. Thicknesses are determined from measurements carried out in both the Si bulk and the capping materials on both sides of the HfO_2 film using the relation $t/\lambda=\ln(I_t/I_0)$, where t is the thickness, λ is the mean free path of the electrons (equal to 140 nm for Si and Ge and to 130 nm for Al_2O_3 at 200 keV), I_t is the integral of the low-loss spectrum (between −3 and 97 eV), and I_0 is the integral of the zero-loss peak (between -3 and 3 eV). For HREM imaging, a LaB_6 JEOL 4000EX microscope dedicated to high resolution (point resolution of 0.17 nm) fitted with a 2000×2000 Gatan multiscan camera is used. All HREM images are recorded on samples oriented in the [110] zone axis of the Si lattice. EELS experiments are performed using an FEI TECNAI F20 or an FEI TECNAI F20-ST. Both are Schottky field emission gun transmission electron microscopes (SFEG-TEM) equipped with a high resolution Gatan imaging filter (HR-GIF 2000), a high angle annular dark field detector (HAADF), and a scanning module. The F20-ST version is modified for better high voltage stability and is fitted with a special high tension tank and a monochromator for better instrumental energy resolution [classically defined as the full width at half maximum (FWHM) of the zero-loss peak in vacuum]. In this study EELS profiles are recorded with an energy resolution of 0.5 eV and a spatial resolution of 0.25 nm (spot size). On the conventional F20 TEM energy resolutions of 0.7–0.8 eV are obtained for the same spatial resolution. EELS line scans are recorded in both directions: from the Si substrate to the capping material and the reverse under the following conditions: spot size of 0.25 nm, camera length of 40 mm, illumination and collection angles of 16 and 4.76 mrad, respectively, energy window of 100 eV between −10 and 90 eV with an energy dispersion of 0.1 eV/channel, number of spectra per scan of 20, spatial distance between two acquisitions of 0.25 nm. All spectra are recorded with the electron beam slightly out of the [110] zone axis of the Si substrate to prevent strong diffraction effects (tilt 6.7° away from the [110] and 2° from the [001] axis). All spectra are corrected for the dark current and gain variations of the charge coupled device (CCD) camera. They are processed using the electronic structure tools software[8] developed within GRAM 32[9] to calculate the single scattering distribution (SSD) spectra. SSD spectra are obtained from experimental spectra by deconvolution of elastic phonon and multiple scattering effects. This is achieved by fitting the experimental zero-loss peak with a multiparameter asymmetric function[10] followed by Fourier-log deconvolution proposed by Johnson and Spence[11] and computed by Egerton.[12] The convergence angular effects are corrected using Egerton's CONCOR software.[12]

III. RESULTS

A. HREM investigations

Theoretical studies carried out on several HfO_2 crystal structures have shown that the electronic properties, i.e., band gap (E_g) and dielectric constant (ε), can vary significantly with the structure.[13,14] Again, this indicates that the crystal structure of the HfO_2 films has to be accurately determined in parallel with their physical properties. For this purpose HRTEM images of the three stacks under study are recorded. Three of them are displayed in Fig. 1. These images are selected out of many. They represent the typical morphology and microstructure of the HfO_2 layers, such as thickness variation and crystallinity. A zoom is superimposed to highlight interface features. Because of very different deposition and postdeposition conditions, important structural differences between the three films are expected. Regarding the morphology, the ALD HfO_2 layers capped with poly-Si or poly-Ge are a little bit thicker than the CVD HfO_2 layer capped with Al_2O_3 (~4 nm against ~3.6 nm in average). Moreover, ALD deposited films show a constant thickness and straight, sharp interfaces with Si/SiO_2 as well as with poly-Si or poly-Ge, whereas the CVD deposited film shows small fluctuations in thickness (± 0.2 nm), and its interfaces with both the substrate and the cap material appear rougher and blurred. This indicates that a better control of the morphology of the dielectric thin film is achieved by using ALD. The SiO_2 layer, deposited to prevent chemical interaction between the substrate and the dielectric, is also very different in the ALD and the CVD samples. It is composed of only three or four atomic layers in the case of the ALD samples, whereas it is several nanometers thick (varying between 1.5 and 3.5 nm) in the case of the CVD samples.

Regarding the microstructure, we observe that the three annealed HfO_2 films are mainly polycrystalline with varying contributions of amorphous zones. The ALD deposited film capped with poly-Ge is almost fully crystallized. In general, its grains are large, but a few zones composed of several small grains can be also observed. As shown in the zoom of Fig. 1(a), some of the grains extend throughout the whole film thickness and laterally on several tens of nanometers. ALD deposited films capped with poly-Si are also rather well crystallized, but they are exclusively composed of small grains ($\varnothing\leqslant10$ nm). This is illustrated in Fig. 1(b), where a lot of disoriented small grains can be distinguished. Some-

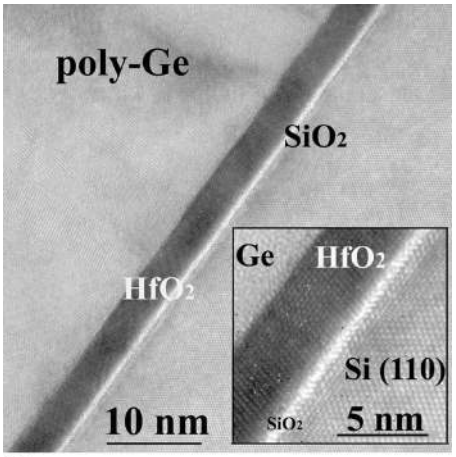

(a)

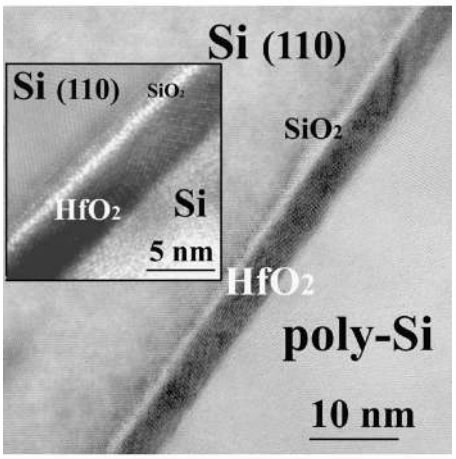

(b)

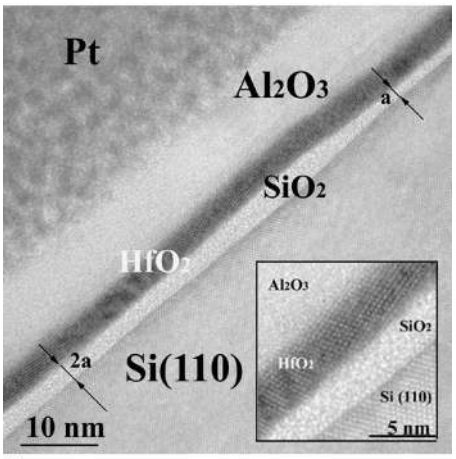

(c)

FIG. 1. HREM images obtained for the three stacks using a JEOL HR-400 kV: (a) ALD $Si/SiO_2/HfO_2/poly\text{-}Ge$, (b) ALD $Si/SiO_2/HfO_2/poly\text{-}Si$, and (c) CVD $Si/SiO_2/HfO_2/poly\text{-}Al_2O_3$. The crystalline nature of the HfO_2 layers and the interfaces with the substrate and the cap material are shown in the insets, respectively.

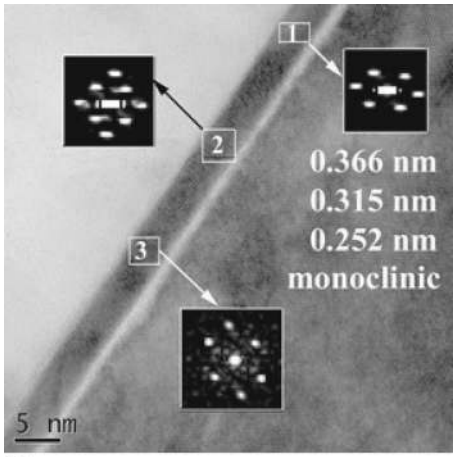

(a)

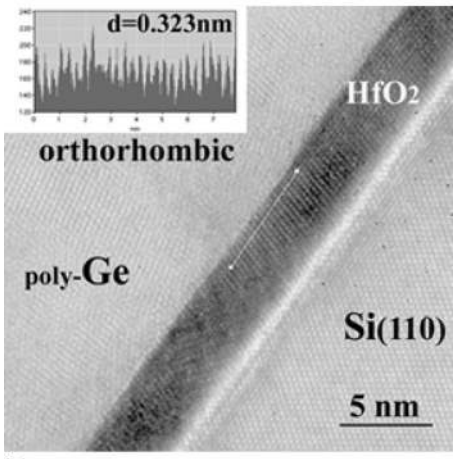

(b)

FIG. 2. Determination of the crystal structure of the HfO_2 layer in the $Si/SiO_2/HfO_2/poly\text{-}Ge$ stack: (a) from fast Fourier transformation analysis and (b) from measurements of the interplane spacing in the real space using Digital Micrograph tools.

times, although imaging of electrically dense materials such as HfO_2 is difficult, Moiré fringes can be distinguished. Since the Moiré fringes are the result of lattice interferences of two disoriented grains, this confirms the nanocrystalline structure of the $Si/SiO_2/HfO_2/poly\text{-}Si$ film in all directions. Finally, it has to be noted that the ALD poly-Si capped film presents some small badly crystallized or amorphous zones. This is confirmed by applying fast Fourier transformation to these zones. In contrast to the high crystallinity of the ALD layers, the CVD HfO_2 films capped with alumina are composed of a mixture of midsized grains with diameters ranging from 5 to 20 nm, interrupted by residual amorphous zones [Fig. 1(c)]. Well crystallized zones are generally observed where the SiO_2 layer is thick, and reciprocally badly crystallized or amorphous zones correspond to zones with a thinner SiO_2 underlayer.

The crystal structure of the HfO_2 layers is determined by analyzing the HREM images by three methods: indexing the electron diffraction patterns calculated from fast Fourier transform (FFT) analysis, measuring interplane spacing in real space, and applying the phase image analysis method of Hytch.[15] Each method is calibrated using measurements obtained on the perfectly oriented Si substrate, far from the $Si-SiO_2-HfO_2$ interface to avoid the region where the Si is stressed. These calibration experiments show that the error bars for the lattice constant determinations are smaller than 2%. In Fig. 2 the results of the FFT (a) and the interplane

TABLE I. Crystal structure of the three HfO_2 films.

	$Si/SiO_2/HfO_2$/poly-Si ALD deposited	$Si/SiO_2/HfO_2$/poly-Ge ALD deposited	$Si/SiO_2/HfO_2$/poly-Al_2O_3 CVD deposited
e^- diffraction patterns from FFT	Orthorhombic (locally amorphous)	Monoclinic (80%), orthorhombic (20%)	Orthorhombic +amorphous
Interplane spacing measurements	Orthorhombic	mono+ortho	Orthorhombic
Phase image analysis (Hytch)	Orthorhombic (amorphous zones)	Monoclinic (small orthorhombic zones)	Orthorhombic +amorphous

spacing (b) method are illustrated. In Table I the crystal structures determined for the three HfO_2 films are summarized.

For the HfO_2 thin films investigated in this study we find that large grains can always be indexed with the monoclinic structures, as reported in the JCPDS database[16] (it is indeed the crystal structure obtained in majority in the Ge capped ALD film). Small grains tend to crystallize in the orthorhombic[17] structure. Thanks to the high precision of the calculation of the crystal structure parameters from HREM images (around 2% as deduced from the calibration experiments), it is possible to discriminate and identify the *Pmnb* orthorhombic structure among the five existing space groups, i.e., *Pbca*, *Pnma*, $Pbc2_1$, $P2_12_12_1$, and *Pmnb*. The most frequent interplane spacings measured in HfO_2 HREM images are $3.14_7 \pm 0.05$ and $3.22_6 \pm 0.05$ Å. The first distance can be attributed either to the [111] interplane spacing of the $P21/a$ or to the *Pmnb* space group of the orthorhombic phase. On the contrary, the second distance can be exclusively attributed to the [002] interplane spacing of the *Pmnb* space group. Hence, since nearly all crystalline zones of the poly-Si capped HfO_2 ALD film and of the Al_2O_3 capped HfO_2 CVD film consist mainly of small grains, their crystal structure is dominated by the *Pmnb* space group of the orthorhombic structure. Several papers focusing on ZrO_2 crystal structures have already indicated that it should be possible to stabilize this structure at ambient pressure, and recently Ram and Mondal[18] reported to have obtained it in ZrO_2 nanoparticles. They conclude that the synthesis at ambient pressure of the ZrO_2 *Pmnb* orthorhombic phase results from the nanometer size of the particles. Taking into account the similarities between the ZrO_2 and the HfO_2 properties, it is not surprising to identify the *Pmnb* orthorhombic structure in our HfO_2 thin films. In the bulk, the most stable HfO_2 structure at atmospheric pressure and temperatures below 1000 °C exhibits the space group $P2_1/c$ of the monoclinic[19] phase also known as baddeleyite. Since the depositions are performed close to ambient pressure and the annealing temperatures are lower than 1000 °C, a monoclinic structure should be expected for all three films. However, it is well known that in thin films metastable structures can be stabilized by stress or grain-size effects.[19–21] Hafnium dioxide films often crystallize into the monoclinic phase, but amorphous and tetragonal HfO_2 phases can also be obtained in samples with high surface to volume ratio.[19]

B. Chemical profiles

The method we use to establish chemical profiles by low-loss spectroscopy is detailed in a previous paper.[22] In summary, it is based on the assumption that each single scattering distribution spectrum of a line scan (SSDL) can be represented by a linear combination of weighted single scattering distribution reference (SSDR) spectra. The reference spectra are recorded for each element/compound beforehand in similar conditions as used for line scan. This method works well for layers with clearly defined phases, but it reaches its limits for layers with composition gradients or heterogeneities because the reference spectrum of a compound A_aB_b is representative of one given stoichiometry and one given crystal structure. To evaluate the spatial resolution of the chemical profiles (delocalization effects), we trace in parallel the zero-loss peak (ZLP) intensity profile, which corresponds to the response of a highly localized interaction process.

In Figs. 3(a) and 3(b) the chemical profiles and the zero-loss peak intensity profiles of the ALD films are shown. Pure HfO_2 is only present in the middle of the films and it extends over less than 3 nm. The Si_{mono}/SiO_2 and SiO_2/HfO_2 interfaces are rather sharp in all cases. The broadening of the chemical profiles at the interfaces is rather due to the thickness of the TEM foil and to the probe broadening than due to the formation of a chemical compound. This is also true for the HfO_2/Ge_{poly} interface since all SSDL can be fitted correctly by a linear combination of the reference spectra. On the contrary, in the case of the $Si_{mono}/SiO_2/HfO_2/Si_{poly}$ stack the spectra in the HfO_2/Si_{poly} interface region cannot be decomposed into a linear combination of Si, SiO_2, and HfO_2 reference spectra. This indicates that there is a chemical interaction between the HfO_2 and the poly-Si cap. The comparison of these spectra to a reference $HfSiO_4$ low-loss spectrum[23] excludes the formation of such a stoichiometric compound. We conclude that an interfacial layer containing Hf, O, and Si atoms is formed, extending on a thickness of about 1.2 ± 0.3 nm.

In the case of the CVD sample, none of the spectra of the line scan recorded across the HfO_2 layer is identical to pure HfO_2. Figure 4(a) represents three typical low-loss spectra recorded across the CVD layer (close to the interfaces and in the middle of the layer) in comparison to a HfO_2 low-loss reference spectrum recorded from a bulk sample.[24] The relative intensity increase of the shoulder at 23 eV from the Si/SiO_2 substrate to the Al_2O_3 cap indicates the existence of a composition gradient across the layer. Two elements/compounds in the CVD sample exhibit plasmons in the energy range of the shoulder or larger. Hence, the mixing of either of these two elements can possibly contribute to the intensity increase and energy shift of this shoulder through-

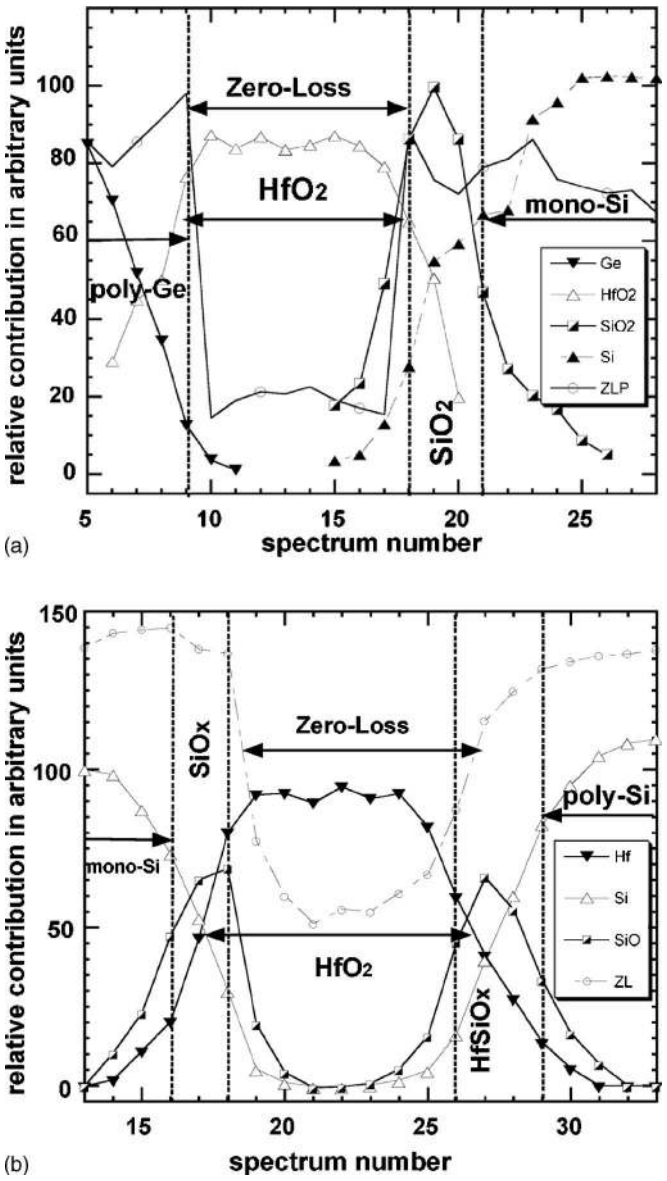

FIG. 3. Chemical and ZLP intensity profiles recorded across the HfO_2 layer of (a) the $Si/SiO_2/HfO_2$/poly-Ge stack and (b) the $Si/SiO_2/HfO_2$/poly-Si stack. Note that the interface of HfO_2 with poly-Ge is sharp, whereas the formation of a Hf-silicate is observed at the interface with poly-Si. Note also that the measurements are done with a spatial resolution of about 0.4 nm (about one monolayer).

out the layer: carbon at 24 eV[12] (coming from the organic precursor used in the deposition process) and alumina at 23 eV[12] (capping). Fortunately, the Al-$L_{2,3}$ core edge, located at 76 eV, is contained in the low-loss acquisition energy window. The absence/presence of this edge allows us to conclude that there is no alumina present in the HfO_2 layer, but only close to the HfO_2/Al_2O_3 interface [see Fig. 4(b)]. To prove the presence of carbon, core loss experiments are performed in the spot mode (electron beam of 3 nm) on the Si substrate and on the HfO_2 layer using a larger collection angle (β=20 mrad). Typical spectra are displayed in Figs. 4(c) and 4(d). They show that traces of carbon are detected in both configurations: on the Si substrate and on the HfO_2 layer; therefore, by comparing the calculated second difference spectra presented in Fig. 4(d), we see that the carbon signal is slightly stronger in the HfO_2 spectrum than in the Si substrate. This indicates that carbon is incorporated in HfO_2. This has been confirmed by performing secondary-ion-mass spectroscopy (SIMS) profiles.

C. Band gap

Several methods exist to determine the band gap from low-loss spectra. In the simple case of wide band gap materials, E_g can be determined by eye inspection of the SSD spectrum. E_g is then defined as the energy corresponding to the first onset observed in the spectrum.[25,26] All the other methods are more sophisticated and are based on Bethe's theory[12] because the transitions close to the band gap have an atomic character (no collective excitations). Bethe's theory states that the SSD spectrum is proportional to the product of the joint density of states (JDOS) and the transfer matrix elements between ground states and excited states for states close to the band gap. Under the assumption that the transfer matrix elements vary slowly with energy, the SSD spectrum is proportional to the JDOS for small energies. Using the effective mass approximation for the valence band (VB) and the conduction band (CB), it has been shown[27] for small collection angles ($k \approx 0$) that several eV above the band gap, the JDOS follows an $I(E)=I_0+c(E-E_g)^{1/2}$ law for a direct band gap and an $I(E)=I_0+c(E-E_g)^{3/2}$ law for an indirect band gap, where I_0 and c are constants, E is the energy loss, and E_g is the band gap value. E_g can be thus determined by fitting the single scattering spectrum using the appropriate function. We will refer to this method as "the fitting method" throughout the paper.

A more reliable and accurate procedure was developed by Rafferty and Brown[28] without requiring *a priori* knowledge of the nature of the gap. Rafferty and Brown found that the experimental spectrum is fitted best by a function of the form $(E-E_{g_m})^n$, if the trial band gap E_{g_m} is equal to the correct band gap E_g. It is assumed that each data point $I_m(E_m^j)$ in the band gap region of the SSD spectrum could be the onset of $(E-E_{g_m})^n$. For each trial band gap E_m^j, the $I_m(E_m^j)$ point is moved to the origin of the coordinate system. Then, a log-log plot of the shifted SSD is drawn and fitted with a line: $Y=A+BX$. The best fit is obtained when the reliability R^2 is maximum. According to Rafferty and Brown, the trial band gap of the best fit is the correct band gap and B (equal to n) is an indicator for the nature of the band gap ($n=1/2$, direct band gap; $n=3/2$, indirect band gap). The weak point of this method is its noise sensitivity since the shifts of the SSD spectra are defined by single data points $I_m(E_{g_m})$.

In this study, the band gaps of the two ALD deposited HfO_2 layers are determined by applying both the fitting and the Rafferty-Brown method. To increase the signal to noise ratio and to reduce the statistical noise for both ALD HfO_2 layers, the pure HfO_2 spectra across the layer are added up to get a noise reduced "SSD sum spectrum." In Figs. 5(a) and 5(b) the results of the band gap determination for the $Si_{mono}/SiO_2/HfO_2/Ge_{poly}$ stack are displayed. For the fitting method we assume a direct band gap and use a fitting law of the form $(E-E_g)^{1/2}$; for Rafferty-Brown the values of n and

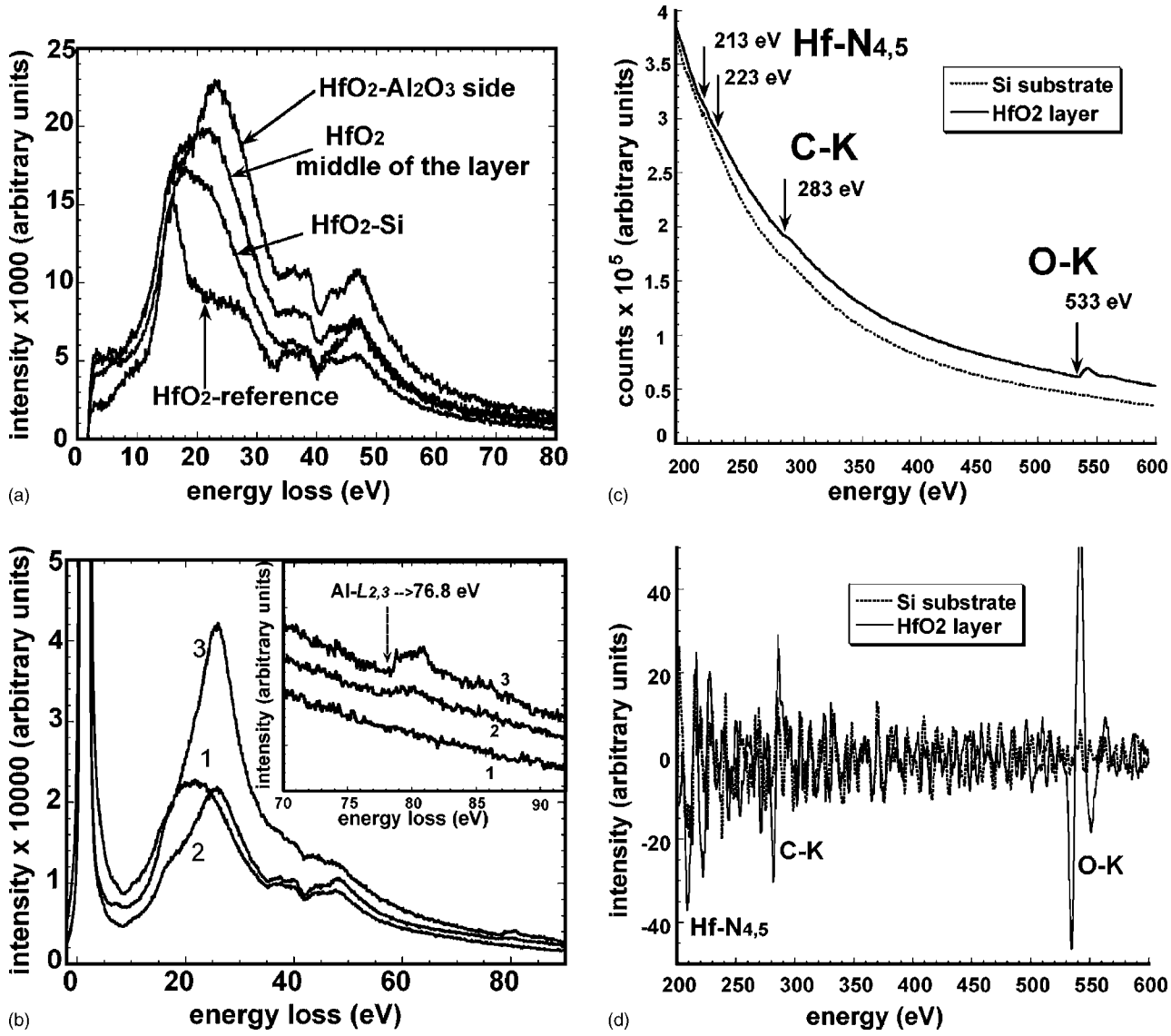

FIG. 4. (a) Comparison of three typical spectra recorded across the CVD HfO_2 layer (close to the interfaces, in the middle of the layer) to a reference HfO_2 low-loss spectrum. (b) Three consecutive spectra recorded close to the HfO_2/Al_2O_3 interface (1: 0.8 nm, 2: 0.4 nm, and 3: on the interface). The absence of the Al-$L_{2,3}$ edge in the spectra allows us to exclude alumina contribution to HfO_2 low-loss spectra. (c) EELS experimental spectra recorded in the 200–600 eV energy range: small traces of carbon are observed in both Si substrate and HfO_2 layer. (d) Calculated second difference spectra corresponding to experimental results of Fig. 4(c): a stronger carbon signal is clearly observed in the HfO_2 layer; this indicates that in addition to carbon contamination, carbon atoms are incorporated in the HfO_2 layer.

R^2 are plotted as a function of the trial band gaps. In the case of the CVD deposited HfO_2 film, we could not sum up over several low-loss spectra to obtain a SSD sum spectrum with reduced noise since each spectrum is different. Thus, we choose a representative spectrum in the middle of the layer and apply exclusively the fitting method. In Table II the band gap values obtained by each method and for all the samples are summarized. We find a very good agreement between the band gaps obtained with the fitting or the Rafferty-Brown method, whereas slight deviations are observed for the nature of the gap. With the Rafferty-Brown method we find 0.6 or 0.7 instead of 0.5. This could indicate that small contributions of indirect transitions occur at the band gap or close to the band gap. Our experimental results show that the HfO_2 layer of the $Si_{mono}/SiO_2/HfO_2/Si_{poly}$ stack exhibits a band gap of 0.6 eV (1.2 eV) higher than that for the HfO_2 layer of the $Si_{mono}/SiO_2/HfO_2/Ge_{poly}$ ($Si_{mono}/SiO_2/HfO_2/Al_2O_{3poly}$), respectively. In the case of the HfO_2/Al_2O_{3poly} film, the difference is, of course, attributed to the carbon content introduced by the precursors in the HfO_2 layer. The most obvious way to explain the band gap difference between the two ALD deposited films is based on the difference in the microstructure and in the crystal structure. A nanocrystallized orthorhombic phase is stabilized for HfO_2/polySi, whereas we find large monoclinic grains in the HfO_2/Ge_{poly} film.

To shed light on the correlation between band gap and crystal structure, we would like to compare our results to literature. Although a lot of experimental and theoretical papers have already reported on the HfO_2 band gap, giving values between 5.1 and 6.3 eV, unfortunately the chemistry and the crystal structure of the samples are rarely indicated. For example, Frandon*et al.*[29] measure a band gap of 5.5 eV by EELS, while Yu *et al.*[30] find 5.25 eV. Since in both cases

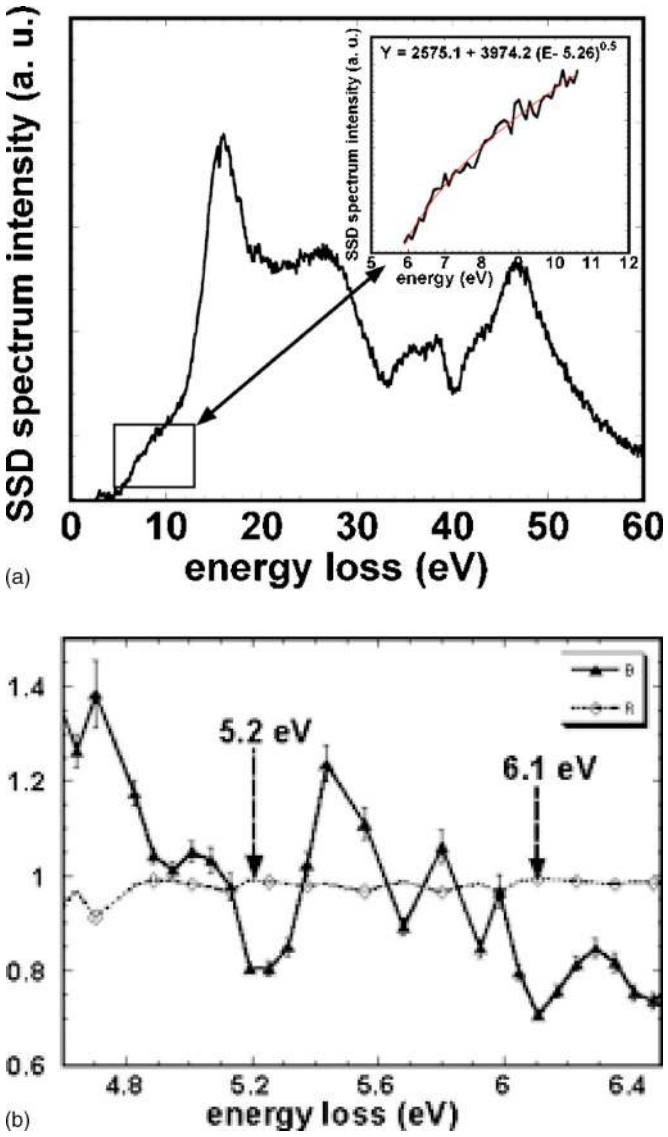

FIG. 5. Band gap determination of the HfO_2 layer in the $Si/SiO_2/HfO_2$/poly-Ge based on (a) the fitting method and (b) the Rafferty-Brown method.

the experiments are performed on pure HfO_2 bulk samples (equilibrium bulk phase), we assume that the samples are crystallized into the monoclinic crystal structure. Balog *et al.*[31] reported a band gap of 5.68 eV for a monoclinic CVD HfO_2 film of 230 nm deposited on a Si substrate measured by ultraviolet spectroscopy (UVS). Modreanu *et al.*[32] found by ellipsometry an optical band gap of 5.8±0.1 eV for an amorphous metal oxide chemical vapor deposition (MOCVD) thin film, whereas a value of 5.5 eV was obtained by Ito *et al.*[33] In terms of theoretical results, GW calculations found a band gap of 5.5 eV for the HfO_2 fluorite phase[34] and band gaps of 5.53, 5.79, and 5.65 eV for the HfO_2 cubic, tetragonal, and monoclinic phases,[14] respectively. These literature values are added to Table II.

Because of the lack of experimental data in the literature for the orthorhombic HfO_2 phase, we restrict the comparison of our results to the data obtained for the monoclinic phase. In this case we find good agreement between our band gap value (5.3±0.5 eV) and the experimental EELS band gap values determined by Yu *et al.*[30] (E_g=5.25 eV) and by Frandon *et al.*[29] (5.5±0.2 eV). On the contrary, in comparison to the UV spectroscopy result (E_g=5.68 eV) of Balog *et al.*,[31] our band gap is about 0.4 eV smaller. It is interesting to notice that the method used by Balog *et al.* to determine the band gap gives actually the first direct transition which is equal to the optical band gap, while with EELS direct and indirect transitions are probed. Nevertheless, in this optical spectrum, one can notice that there is already a small intensity increase at 5.25 eV, which could be due to an indirect band gap. This is another indication that the electronic structure of HfO_2 close to the band gap is rather complicated, leading to direct and indirect transitions which are close in energy.

The complexity of the HfO_2 band diagram is confirmed by electronic structure calculations. Since Nishitani *et al.*[14] have used the GW code, known today as the most powerful approach, we comment our band gaps only in comparison to their results. The analysis of their monoclinic phase band diagram shows that both valence band (VB) edge and conduction band (CB) edge are flatbands. The band gap corresponds to an indirect transition from $\Gamma \rightarrow B$ (5.65 eV) followed closely in energy by a direct transition $B \rightarrow B$ (5.9 eV). This energy difference between the indirect band gap and the first direct transition is in good agreement to the difference between EELS results (indirect contributions) and UV results (direct transition). Although we can match theoretical and experimental data very well qualitatively, we find differences comparing absolute values: the EELS band gap of this work (5.3 eV) is 0.35 eV lower than the GW band gap (5.65 eV). One possibility to explain this difference of

TABLE II. Band gap of the three HfO_2 layers (first two rows). Comparison to experimental data and *ab initio* values from literature (rows 3 and 4).

	$Si/SiO_2/HfO_2$/poly-Si ALD-orthorhombic	$Si/SiO_2/HfO_2$/poly-Ge ALD-monoclinic	$Si/SiO_2/HfO_2/Al_2O_3$ CVD-contamination
Fitting method $(E-E_g)1/2$	5.8±0.5 eV	5.3±0.5 eV	4.6±0.7 eV
Rafferty-Brown $n(E)R(E)$	5.9±0.85 eV	5.3±0.8 eV	
Literature (experiments)		5.25 eV[36]–5.65 eV[37]	
Literature (theoretical results)	5.8 eV[21]	5.65 eV[21]	

0.3 eV are excitonic effects which are not included in the theoretical approach. Concerning our VEELS results, it seems surprising at a first glance, in the light of this interpretation, to find a direct band gap with indirect contributions instead of an indirect band gap. To explain these results we need to take into account the zero-loss width (ZLW) of the electron beam (0.6 eV). It is wide enough to excite indirect and direct transitions at roughly the same energy. Under our angular conditions (large illumination angle α and small β, i.e., electrons with small k_{perp} values), indirect transitions are underestimated in comparison to direct transitions. This means that VEELS analysis is capable of giving relevant information on the band gap and on the electronic structure of complex dielectric materials.

IV. CONCLUSION

Three HfO_2 films deposited on a $Si(110)/SiO_2$ substrate by ALD and CVD and capped with polycrystalline Si, Ge, or Al_2O_3 were studied. For each sample, chemistry and crystal structure are determined by analyzing the valence electron scattering response and high resolution electron microscopy images, respectively. In the three cases, chemistry and crystal structure are very different as a consequence of the process and the cap material. These results allow us to correlate the variations of the band gap determined by the Rafferty-Brown or the "fitting" method to the crystal structure and morphology of the films. This study shows again that valence electron energy loss spectroscopy is a powerful and relevant tool to access structural, chemical, and electronic information at a subnanometer scale when it is performed in a high resolution (spatial and energy) transmission electron microscope.

ACKNOWLEDGMENTS

The authors thank T. Epicier (MATEIS-INSA Lyon) for his assistance with HREM image processing, W. Saikaly (TECSEN-CP2M Marseille) for his help for core-loss EELS analysis, S. Lhostis for providing sample wafers and C. Wyon for helpful discussions.

[1]G. D. Wilck, R. M. Wallace, and J. M. Anthony, J. Appl. Phys. **87**, 484 (2000).
[2]P. E. Batson, Ultramicroscopy **59**, 63 (1995).
[3]M. P. Augustin, G. Bersuker, B. Foran, L. A. Boatner, and S. Stemmer, J. Appl. Phys. **100**, 024103 (2006).
[4]D. A. Muller, T. Sorsch, S. Moccio, F. H. Baumann, K. Evans-Lutterodt, and G. Timp, Nature (London) **399**, 758 (1999).
[5]N. Ikarashi and K. Manabe, J. Appl. Phys. **94**, 480 (2003).
[6]T. Topuria, N. D. Browning, and Z. Ma, Appl. Phys. Lett. **83**, 4432 (2003).
[7]M. C. Cheynet and T. Epicier, Philos. Mag. **84**, 1753 (2004).
[8]L. Denoyer and R. French, Electronic Structure Tool (EST) software, Deconvolution and Entropy Consulting, 755 Snyder Hill Road, Ithaca, NY, 1996 (http://www.deconvolution. com/), developed under GRAM 32, Galactic Industries, 325 Main Street, Salem, NH 03079, 1996.
[9]GRAM 32, software developed by Galactic Industries, 325 Main Street, Salem, NH 03079, 1996.
[10]D. Dorneich, R. H. French, H. Müllejans, S. Loughin, and M. Rhüle, J. Microsc. **191**, 286 (1998).
[11]D. W. Johnson and J. C. H. Spence, J. Phys. D **7**, 771 (1974).
[12]R. Egerton, *Electron Energy-Loss Spectroscopy in the Electron Microscope*, 2nd ed. (Plenum, New York, 1996).
[13]X. Zhao and D. Vanderbilt, Phys. Rev. B **56**, 233106 (2002).
[14]K. Nishitani, P. Rinke, P. Eggert, S. J. Hashemifar, P. Kratzer, and M. Scheffler, Phys. Rev. B (unpublished).
[15]M. J. Hytch, Microsc. Microanal. Microstruct. **8**, 41 (1997).
[16]X-Ray Powder Diffraction Files JCPDS-ICCD (Joint Committee on Powder Diffraction Standards-International Centre for Diffraction Data, Swarthmore, PA, 1999.
[17]J. Tang, M. M. Kai, Y. Kobayashi, S. Endo, O. Shimomura, T. Kikegawa, and T. Ashida, Geophys. Monogr. **101**, 401 (1998).
[18]S. Ram and A. Mondal, Phys. Status Solidi A **201**, 696 (2004).
[19]S. V. Ushakov *et al.*, Phys. Status Solidi B **241**, 2268 (2004).
[20]R. C. Garvie, J. Phys. Chem. **82**, 218 (1978).
[21]A. A. Demkov, Phys. Status Solidi B **226**, 57 (2001).
[22]S. Pokrant, M. C. Cheynet, S. Jullian, and R. Pantel, Ultramicroscopy **104**, 233 (2005).
[23]M. Floyd, R. W. Carpenter, S. K. Dey, S. Marcus, H. de Waard, and C. Werkhoven, Microsc. Microanal. **9**, 466 (2003).
[24]C. C. Ahn, O. Krivanek, R. P. Burgner, M. M. Disko, and P. R. Swann, *EELS Atlas* (Gatan, Warrendale, PA, 1983).
[25]L. A. J. Garvie, P. Rez, J. R. Alvarez, and P. R. Buseck, Solid State Commun. **106**, 303 (1998).
[26]S. Lazar, G. A. Botton, M. Y. Yu, F. D. Tichelaar, and H. W. Zandbergen, Ultramicroscopy **96**, 535 (2003).
[27]J. Bruley and L. M. Brown, in *Analytical Electron Microscopy Workshop, Proceeding*, edited by G. W. Lorimer (The Institute of Metals, London, 1997).
[28]J. Rafferty and L. M. Brown, Phys. Rev. B **58**, 10326 (1998).
[29]J. Frandon, B. Rousseau, and F. Pradal, Phys. Status Solidi B **98**, 379 (1980).
[30]H. Y. Yu *et al.*, Appl. Phys. Lett. **81**, 376 (2002).
[31]M. Balog, M. Schieber, M. Michman, and S. Patai, Thin Solid Films **41**, 247 (1977).
[32]M. Modreanu, Proc. SPIE **4876**, 1236 (2002).
[33]T. Ito, M. Maeda, K. Nakamura, H. Kato, and Y. Ohki, J. Appl. Phys. **97**, 054104 (2005).
[34]J. Dabrowski, V. Zavodinsky, and A. Fleszar, Microelectron. Reliab. **41**, 1093 (2001).